


Carrier Distribution Control in van der Waals Heterostructures of MoS₂ and WS₂ by Field-Induced Band-Edge Engineering

Mina Maruyama^{1,*}, Kosuke Nagashio², and Susumu Okada^{1,†}

¹*Department of Physics, Graduate School of Pure and Applied Sciences, University of Tsukuba, 1-1-1 Tennodai, Tsukuba, Ibaraki 305-8571, Japan*

²*Department of Materials Engineering, Graduate School of Engineering, The University of Tokyo, 7-3-1 Hongo, Bunkyo-ku, Tokyo 113-8656, Japan*

 (Received 14 July 2020; revised 26 August 2020; accepted 17 September 2020; published 16 October 2020; corrected 13 January 2021)

The electronic properties of van der Waals heterostructures composed of MoS₂ and WS₂ under a perpendicular electric field are studied in terms of field strength, electron doping concentration, and interlayer stacking arrangement based on the density-functional theory. The calculation results show that accumulated carrier distribution can be controlled by tuning the field direction, field strength, and doping concentration. The electron is localized on the MoS₂ layer on the positively charged electrode side under a strong positive field with a low doping concentration, whereas they are extended throughout both the MoS₂ and WS₂ layers under a strong negative field. Stacking misorientation between the layers further enhances the electron localization under a positive field and delocalization under a strong negative field. The stacking arrangement and electric field allow additional tuning of the electronic properties of van der Waals heterostructures.

DOI: [10.1103/PhysRevApplied.14.044028](https://doi.org/10.1103/PhysRevApplied.14.044028)

I. INTRODUCTION

Electric fields are widely used to control the physical properties of solids, thin atomic films, and molecules in numerous fields of pure and applied sciences [1]. Unusual physical properties have been induced in materials by applying external electric fields. These properties depend on the field strength, the carrier concentration, the constituent elements, and their geometries. The high carrier density of ionic liquid electrolytes with an electric double layer [2–4] results in room-temperature ferromagnetism in Co-doped TiO₂ [5], high carrier mobility at low power in organic semiconductors [6], and superconductivity in several insulators [7–10]. Bilayer graphene with an *AB* stacking arrangement exhibits a metal-semiconductor transition under a perpendicular electric field [11–16]. The band gap of such bilayer graphene is approximately proportional to the weak field and saturates at 0.27 eV at 0.06 V/nm [15,16]. It has been predicted that bilayer graphene returns to the metallic phase under a strong field, the carrier of which is distributed along the graphene sheet and in the vacuum spacing with a nearly free electron nature [16–18].

Atomic layered materials have been attracting considerable attention because their well-controlled two-dimensional electron systems display unusual electronic

properties that depend on the constituent elements of the layers and their stacking arrangement [19]. Atomic layered materials could play a role as building blocks in the construction of hierarchical structures, which are known to be van der Waals structures, by the stacking of adequate layers in appropriate manners. It has been well established that the physical properties of hierarchical structures of layered materials exceed the simple superposition of those of the constituent layers. Graphene possesses a Dirac cone at the Fermi level and the *K* point. Bilayer graphene exhibits an interesting variation of these electronic structures, which depends on the interlayer stacking arrangement [20–23]. Thermal diffusivity between graphene layers is substantially deteriorated by twisting the layers [24]. Layered hierarchical structures composed of heterogeneous constituent layers also display diversity of their physical properties, which depend on the constituent layers and their stacking arrangements [25,26]. Transition-metal dichalcogenides (TMDCs) are representative atomic layer materials that can form hierarchical layered structures with large structural variation. TMDCs with semiconducting electronic properties allow the band-edge alignment of van der Waals heterostructures, whether they are type-I or type-II semiconductors, to be tuned because of their dependence on the constituent layers and the stacking arrangement [27–34].

The application of an external electric field to van der Waals hierarchical structures causes them to exhibit fascinating physical phenomena that are unexpected in the

*mmaruyama@comas.frsc.tsukuba.ac.jp

†sokada@comas.frsc.tsukuba.ac.jp

absence of the applied field. Bilayer graphene with twisted interlayer stacking arrangements under particular magic angles is a superconductor and a strange metal under an applied electric field [35–37]. We demonstrate that for bilayer MoS₂ with twisted stacking under an applied electric field, one of the layers acts as a screening layer upon carrier doping. These findings imply that the constituent elements of the layers further modulate the electronic properties of van der Waals layered structures under an applied electric field, in terms of the band-edge offset and interlayer interactions [38]. Knowledge of the electronic properties of van der Waals heterostructures under an applied electric field is important for practical applications of semiconducting technologies.

Accordingly, in this work, we aim to investigate the electronic properties of van der Waals heterostructures of MoS₂ and WS₂ under a perpendicular electric field from dual-gate electrodes. The interlayer stacking arrangement, field strength, and carrier concentration of the heterostructures are studied using the density-functional theory (DFT) with the effective-screening-medium (ESM) method. Our calculations show that the carrier distribution in the MoS₂/WS₂ heterostructures is sensitive to the field strength, field direction, carrier concentration, and interlayer stacking arrangement.

II. CALCULATION METHOD

All calculations are conducted using the program package STATE [39,40], based on DFT [41,42]. To express the exchange-correlation potential energy between interacting electrons, we use the generalized gradient approximation (GGA) with the Perdew-Burke-Ernzerhof (PBE) functional [43,44]. Because of the GGA-PBE functional, the conduction-band edge of constituent TMDCs is underestimated. Furthermore, it should be noted that the band offset of the van der Waals heterostructures depends on the treatment of the many-body effects, such as quasiparticle approaches and hybrid functionals [45]. Therefore, the results shown in this work give a qualitative insight into the carrier accumulation in MoS₂/WS₂ heterostructures. The weak dispersive interaction between MoS₂ and WS₂ layers is treated using the van der Waals density functional vdW-DF2 with the C09 exchange-correlation functional [46,47]. The interactions between valence electrons and ions are described by ultrasoft pseudopotentials [48]. The valence wave functions and the deficit charge density are expanded in terms of plane-wave basis sets with cutoff energies of 25 and 225 Ry, respectively. The atomic structures of the TMDCs are fully optimized until the force acting on each atom is less than 1.33×10^{-3} Hartree/Bohr under their experimental lattice parameter of $a_0 = 0.315$ nm. Integration over the Brillouin zone is carried out using equidistant meshes of $20 \times 20 \times 1\mathbf{k}$ - and $8 \times 8 \times 1\mathbf{k}$ -points for MoS₂/WS₂ with *AB* and twisted

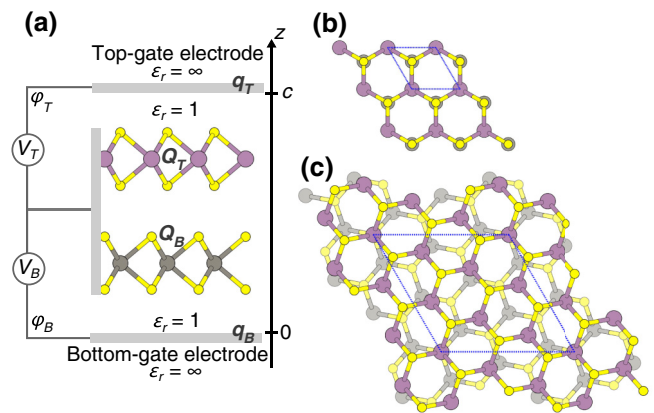


FIG. 1. (a) A structural model of a dual-gate field-effect transistor of MoS₂/WS₂ van der Waals heterostructures with (b) *AB* and (c) twisted interlayer stacking arrangements. The gray rectangles denote the top- and bottom-gate electrodes with infinite permittivity. V_T and V_B are the top- and bottom-gate voltages, respectively, which determine the electrostatic potentials of the top gate, ϕ_T , and the bottom gate, ϕ_B , respectively. The purple, gray, and yellow circles indicate Mo, W, and S atoms, respectively. The blue dotted rectangles denote the lateral unit cell of the MoS₂/WS₂ heterostructures.

stacking arrangements, respectively. The external electric field and excess carriers on each heterostructure are treated using the ESM method (Fig. 1) [49]. During the electronic structure calculations under an electric field and with excess carriers, the geometric structures of the heterostructures are fixed to their optimized structures obtained under zero-electric-field and neutral conditions. The maximum force under the highest electric field with the highest carrier concentration is 2.6×10^{-3} Hartree/Bohr, which is too small to cause substantial structural modulation.

III. STRUCTURAL MODEL

Each MoS₂/WS₂ van der Waals heterosheet is sandwiched by top and bottom gate electrodes that are simulated by a planar ESM with an infinite relative dielectric constant separated by a vacuum spacing of 0.6 nm, resulting in dual-gate field-effect transistors of MoS₂/WS₂ heterostructures [Fig. 1(a)]. A perpendicular electric field with respect to the MoS₂/WS₂ sheet is controlled by the electrostatic potential difference between the top and bottom gate electrodes and the carrier concentration in the sheets is tuned by the electrostatic potential at the middle of the top- and bottom-gate electrodes. For the interlayer stacking arrangement of the heterostructures, we consider *AB* and twisted (twist angle $\theta = 38^\circ$) arrangements [Figs. 1(b) and 1(c), respectively] to investigate the influence of interlayer stacking on carrier accumulation and depression in the heterosheets. Note that the electronic structure of twisted MoS₂/WS₂ with an angle of 38° is qualitatively the same as that with 27° (see the Supplemental Material

[50]). Thus, MoS₂/WS₂ with an angle of 38° may represent the qualitative properties of the carrier accumulation in terms of their large twist angles [51]. The optimal inter-layer spacings of the heterostructures of MoS₂ and WS₂ are 0.30 and 0.33 nm for the *AB* and twisted arrangements, respectively.

IV. RESULTS

Figure 2 shows the distributions of electron accumulation and depression normal to the MoS₂/WS₂ heterostructure with an *AB* stacking arrangement under strong (± 1.0 V/nm), weak (± 0.1 V/nm), and zero electric fields at high ($10^{14}/\text{cm}^2$) and low ($10^{13}/\text{cm}^2$) electron-doping concentrations. Note that the electric field and carrier density considered here are relevant to those realized in experiments [52,53]. The carrier distribution is calculated by determining the difference between the valence charge density of heterostructures under an electric field with electron doping and that under an electric field without excess electrons. The distribution depends strongly on the electric field and the doping concentration. Under a zero or weak electric field with a low doping concentration, the electron distribution in MoS₂ is approximately 10% higher than in WS₂, irrespective of the field direction. These results indicate that the band-edge offset between MoS₂ and WS₂ primarily affects the electron accumulation in the MoS₂/WS₂ heterostructure. Under a strong positive electric field with a low doping concentration, 73% of the electrons are accommodated in the MoS₂ layer. A large band-edge offset between MoS₂ and WS₂ leads

to a higher electron density on the MoS₂ layer in the MoS₂/WS₂ heterostructure than that of a MoS₂ layer at the positive-gate side of a bilayer MoS₂ dual-gate FET, where 57% of the electrons are distributed [38]. Accordingly, under the positive electric field, the WS₂ layer acts as a good screening layer against the external field. Conversely, under a strong negative field with a low doping concentration, the electrons are delocalized throughout the layers. At high electron doping, the electron substantially spills over the WS₂ layer, resulting in a symmetric electron distribution even though the sheet consists of MoS₂ and WS₂. Although an asymmetric electron distribution is retained under the strong positive field, the electrons also spill over to WS₂, causing a decrease of the electron concentration on the MoS₂ layer. Therefore, the carrier distribution in the heterostructure is sensitive to the field direction, field strength, and carrier concentration, indicating that the electronic structure of the heterostructure under an applied electric field plays a crucial role in determining the electron accommodation.

The electron distribution also depends on the inter-layer stacking arrangement. Figure 3 shows the distribution of the electron accumulation and depression normal to the MoS₂/WS₂ heterostructure with a twisted stacking arrangement under an electric field and electron doping. As in the case of the MoS₂/WS₂ heterostructure with the *AB* stacking arrangement, the electron accommodation is sensitive to the field direction, field strength, and electron doping concentration. In addition, the stacking misorientation further increases the electron concentration in the MoS₂ layer under the positive electric field and weak

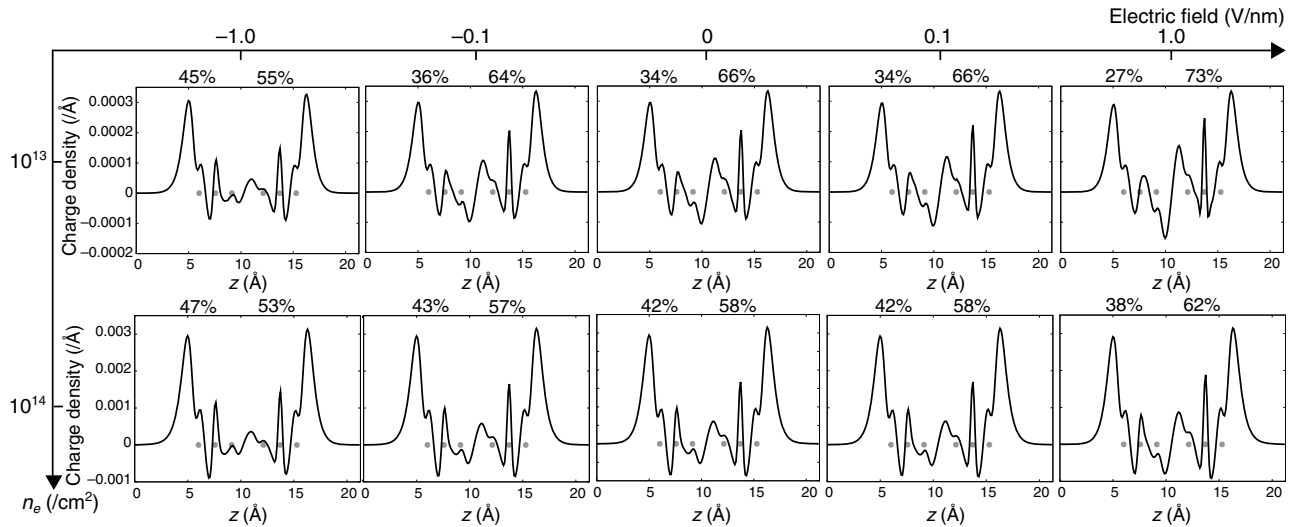


FIG. 2. The accumulated electron distribution as a function of the z axis of a van der Waals heterostructure consisting of MoS₂ and WS₂ with an *AB* stacking structure under strong (± 1.0 V/nm), weak (± 0.1 V/nm), and zero electric fields with high ($10^{14}/\text{cm}^2$) and low ($10^{13}/\text{cm}^2$) doping concentrations. Positive and negative values correspond to the regions where electron accumulation and depression occur, respectively. The numerical values above each panel indicate the carrier ratio accommodated in the WS₂ and MoS₂ layers. The gray points denote atomic positions. In each panel, the left- and right-hand sets of three points correspond to WS₂ and MoS₂ layers, respectively.

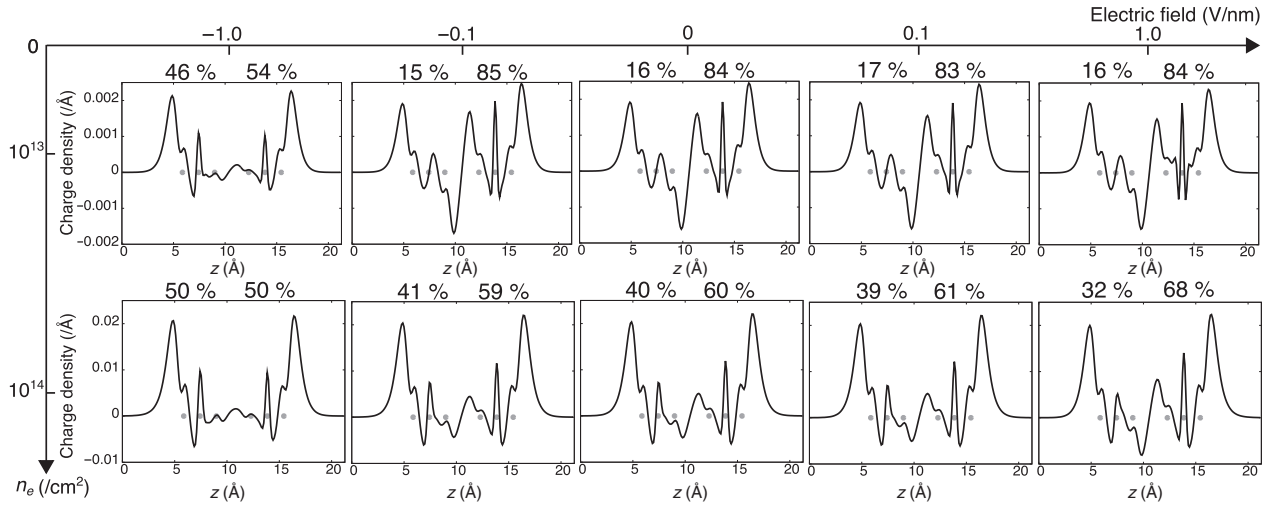


FIG. 3. The accumulated electron distribution as a function of the z axis of the van der Waals heterostructure consisting of MoS_2 and WS_2 with a twisted stacking structure under strong (± 1.0 V/nm), weak (± 0.1 V/nm), and zero electric fields with high ($10^{14}/\text{cm}^2$) and low ($10^{13}/\text{cm}^2$) doping concentrations. Positive and negative values correspond to the regions where electron accumulation and depression occur, respectively. The numerical values above each panel indicate the carrier ratio accommodated in WS_2 and MoS_2 layers. The gray points denote atomic positions. In each panel, the left- and right-hand sets of three points correspond with WS_2 and MoS_2 layers, respectively.

negative electric field compared with that for the heterostructure with the AB stacking arrangement. Over 80% of electrons are localized on MoS_2 under a strong positive field and weak electron doping. With increasing doping concentration, the electron density in WS_2 increases, but 61% and 68% of electrons are still distributed on the MoS_2 layer under weak and strong fields, respectively. Under the weak negative field with a low electron doping concentration, the electrons are highly localized on the MoS_2 layer compared with that in the case of MoS_2/WS_2 with AB stacking. For the strong negative field, the electrons are distributed throughout the layers, showing an approximately symmetric distribution with respect to the layers. Indeed, under a strong field with a high doping concentration, the electrons are equally distributed on the MoS_2 and WS_2 layers.

V. DISCUSSION

As pointed out, the characteristics of the electron distribution of the MoS_2/WS_2 heterostructures under an applied field are associated with their band-edge alignment under the electric field. Figure 4 shows an energy diagram of the electron states of heterostructures with AB and twisted stacking arrangements around the band gap under strong positive and negative (± 1.0 V/nm) electric fields, together with that under the zero electric field. The heterostructure consisting of MoS_2 and WS_2 has type-II band-edge alignment with band gaps of 1.27 and 1.40 eV for the heterostructures with AB and twisted stacking structures, respectively. The band gap of the heterostructures increases with a decreasing electric field because of their

type-II band-edge alignment. For MoS_2/WS_2 with AB stacking, the band gap is wider by 0.07 eV and narrower by 0.12 eV under negative and positive electric fields, respectively, compared with the band gap without an applied electric field. For MoS_2/WS_2 with twisted stacking, the band gap is wider by 0.15 eV and narrower by 0.19 eV under negative and positive electric fields, respectively, compared with the band gap of this structure without an applied electric field. The positive electric field enhances the offset of the conduction-band edges of MoS_2 and WS_2 in the heterostructure. The conduction-band edge localized on MoS_2 is deeper than the lowest unoccupied state associated with the WS_2 layer. Therefore, the doped electrons are primarily accommodated in the MoS_2 layer for the heterostructures with AB and twisted stacking structures.

Under the negative electric field, the conduction-band-edge offset between MoS_2 and WS_2 is substantially suppressed. For the AB stacking, the conduction-band edge is slightly deeper by 0.13 eV than the lowest unoccupied state associated with the WS_2 . Furthermore, the suppression of the band-edge offset also causes interlayer hybridization, leading to the extended nature of the wave function of the conduction-band edge. For the twisted stacking, the conduction-band edge is slightly deeper by 20 meV than the lowest unoccupied state associated with the WS_2 layer. Interestingly, in sharp contrast to the AB stacking, the conduction-band edge of the twisted stacking retains its localized nature on the MoS_2 layer, even though the state has approximately the same eigenvalue compared to that of the lowest unoccupied states associated with the WS_2 layer. As a result, the electrons are accommodated in both

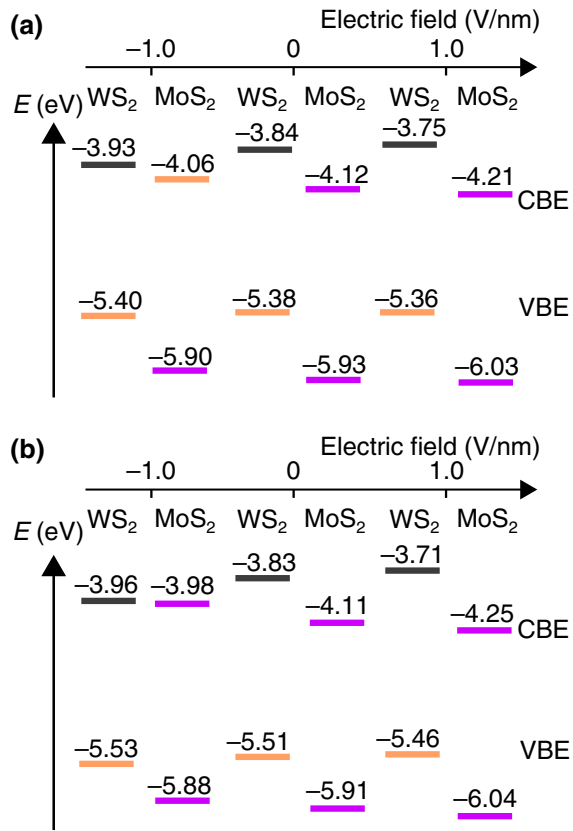


FIG. 4. The energy diagram of the electronic states near the band gap of the MoS₂/WS₂ van der Waals heterostructure with (a) *AB* and (b) twisted stacking structures under strong negative and positive electric fields. The band edges of the heterostructures under the zero electric field are also listed in each figure. The purple, gray, and orange levels indicate the electron states localized on the MoS₂ layer at the *K* point, localized on the WS₂ layer at the *K* point, and distributed on both layers at the Γ points or the middle of the *K*- Γ line, respectively. CBE and VBE indicate conduction and valence band edges, respectively.

the MoS₂ and the WS₂ layers. In particular, at high doping concentration, the doped electrons exhibit a symmetric distribution with respect to these layers. Therefore, the perpendicular electric field can continuously control the band-edge offset of heterogeneous van der Waals materials, leading to further variation of the electronic properties of the heterostructures. To provide further physical insight into the carrier accumulation, we investigate the wavefunction distribution of the MoS₂/WS₂ heterostructures in terms of their interlayer stacking and the external electric field. Figure 5 shows the squared wave function of the conduction-band edge of MoS₂/WS₂ heterostructures with *AB* and twisted stacking arrangements under perpendicular electric fields. For the MoS₂/WS₂ heterostructure with an *AB* stacking arrangement under a negative electric field, the conduction-band edge shows strong hybridization between

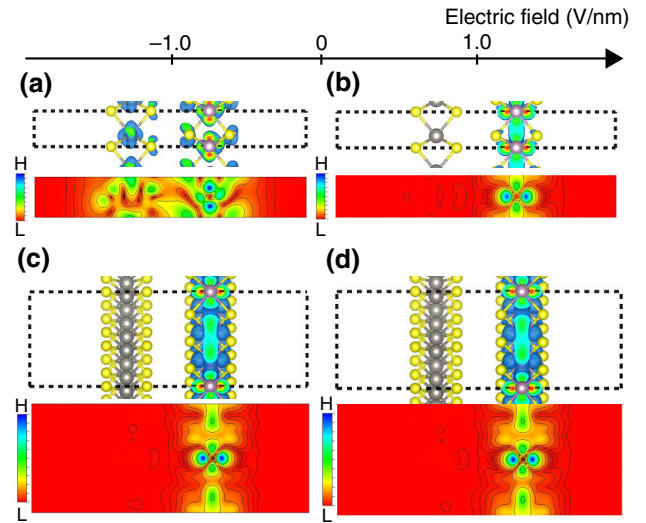


FIG. 5. Isosurfaces and contour plots of the squared wave function of the conduction-band edge of MoS₂/WS₂ van der Waals heterostructures with *AB* stacking under strong (a) negative and (b) positive electric fields and with the twisted stacking arrangement under strong (c) negative and (d) positive electric fields. The purple, gray, and yellow circles indicate Mo, W, and S atoms, respectively. The gray dotted rectangles denote the lateral unit cell of MoS₂/WS₂ van der Waals heterostructures.

MoS₂ and WS₂, because the conduction-band edge is associated with the valley located between the *K* and Γ points [Fig. 5(a)]. According to the wave-function hybridization, the accumulated electrons are extended throughout both layers, even though the band edge is separated from the lowest unoccupied states associated with the WS₂ layers. For the MoS₂/WS₂ heterostructure with a twisted stacking arrangement, in contrast to the case of the *AB* stacking arrangement, the conduction-band edge retains its localized nature on MoS₂ [Fig. 5(c)], owing to the interlayer stacking misorientation, which suppresses the interlayer orbital overlap. However, injected electrons are simultaneously accommodated in the MoS₂ and WS₂ layers, exhibiting an extended nature through the MoS₂/WS₂ heterostructure, because of the nearly degenerate band edges of the MoS₂ and WS₂ layers.

Under a positive electric field, the conduction-band edge is primarily distributed on the MoS₂ layer and was substantially deeper than the lowest unoccupied state associated with the WS₂ layer for both stacking arrangements. Therefore, injected electrons are localized on the MoS₂ layer. By carefully investigating the wave-function distribution, we can further provide physical insights into the enhancement of the electron localization in the heterostructure with the twisted arrangement: the conduction-band edge of the heterostructure with twisted stacking is highly localized on the MoS₂ layer [Fig. 5(d)], whereas that with *AB* stacking has a small but finite amplitude in the WS₂ layer, demonstrating its hybridized nature [Fig. 5(b)]. Therefore,

the enhanced electron localization on the MoS₂ layer in the heterostructure with twisted stacking is ascribed to the highly localized nature of the wave function of the conduction-band edge. Furthermore, the absence of the interlayer hybridization in the twisted stacking arrangement also causes a substantial shift of the conduction-band edge under the positive and negative electric fields.

These results corroborate that the conduction-band-edge alignment of the constituent layers under the external electric field and the interlayer wave-function hybridization by the stacking orientation determined the electron accumulation in the van der Waals heterostructures of TMDCs. This means that the stacking misorientation could be an additional parameter to control the carrier distribution in van der Waals heterostructures under a perpendicular electric field.

VI. CONCLUSION

Using DFT with the ESM method, we investigate the electronic properties of van der Waals heterostructures consisting of MoS₂ and WS₂ under a perpendicular electric field, in terms of the field strength, field direction, doping electron concentration, and interlayer stacking arrangement, in order to provide a theoretical insight into the microscopic mechanism of electron accumulation in dual-gate field-effect transistors with van der Waals heterostructures. Our calculations show that the accumulated carrier distribution can be controlled by tuning the field direction, field strength, and doping concentration. The electrons are localized on the MoS₂ layer under a strong positive field with a low doping concentration, whereas they are extended throughout the layers under a strong negative field. Stacking misorientation between the layers further enhances the electron localization under a positive field at a low doping concentration. Under a strong negative field, the injected electrons are completely delocalized throughout the layers with a twisted stacking arrangement. The characteristic electron distribution in van der Waals heterostructures is ascribed to the conduction band-edge offset of the constituent layers and their spatial distribution, which can be tuned by controlling the field direction, the field strength, and the interlayer stacking arrangement.

ACKNOWLEDGMENTS

We thank the Japan Science and Technology Agency (JST) Core Research for Evolutional Science and Technology (CREST) program (Grants No. JPMJCR1532 and No. JPMJCR1715), the Japan Society for the Promotion of Science (JSPS) Grants-in-Aid for Scientific Research (KAKENHI) (Grants No. JP20H05664, No. JP20K05253, No. JP20H02080, No. JP20H00316, No. JP19H00755, No. JP17H01069, and No. JP16H06331), the Joint Research Program on Zero-Emission Energy Research, the Institute of Advanced Energy, Kyoto University, and the University

of Tsukuba Basic Research Support Program (S). Parts of the calculations were performed on an NEC SX-Ace at the Cybermedia Center, Osaka University.

-
- [1] C. H. Ahn, A. Bhattacharya, M. Di Ventra, J. N. Eckstein, C. D. Frisbie, M. E. Gershenson, A. M. Goldman, I. H. Inoue, J. Mannhart, A. J. Millis, *et al.*, Electrostatic modification of novel materials, *Rev. Mod. Phys.* **78**, 1185 (2006).
 - [2] M. Armand, F. Endres, D. R. MacFarlane, H. Ohno, and B. Scrosati, Ionic-liquid materials for the electrochemical challenges of the future, *Nat. Mater.* **8**, 621 (2009).
 - [3] R. Kötz and M. Carlen, Principles and applications of electrochemical capacitors, *Electrochim. Acta* **45**, 2483 (2000).
 - [4] A. S. Dhoot, J. D. Yuen, M. Heeney, I. McCulloch, D. Moses, and A. J. Heeger, Beyond the metal-insulator transition in polymer electrolyte gated polymer field-effect transistors, *Proc. Natl. Acad. Sci. USA* **103**, 11834 (2006).
 - [5] Y. Yamada, K. Ueno, T. Fukumura, H. T. Yuan, H. Shimotani, Y. Iwasa, L. Gu, S. Tsukimoto, Y. Ikuhara, and M. Kawasaki, Electrically induced ferromagnetism at room temperature in cobalt-doped titanium dioxide, *Science* **332**, 1065 (2011).
 - [6] S. Ono, S. Seki, R. Hirahara, Y. Tominari, and J. Takeya, High-mobility, low-power, and fast-switching organic field-effect transistors with ionic liquids, *Appl. Phys. Lett.* **92**, 103313 (2008).
 - [7] K. Ueno, S. Nakamura, H. Shimotani, A. Ohtomo, N. Kimura, T. Nojima, H. Aoki, Y. Iwasa, and M. Kawasaki, Electric-field-induced superconductivity in an insulator, *Nat. Mater.* **7**, 855 (2008).
 - [8] J. T. Ye, S. Inoue, K. Kobayashi, Y. Kasahara, H. T. Yuan, H. Shimotani, and Y. Iwasa, Liquid-gated interface superconductivity on an atomically flat film, *Nat. Mater.* **9**, 125 (2010).
 - [9] A. T. Bollinger, G. Dubuis, J. Yoon, D. Pavuna, J. Misewich, and I. Božović, Superconductor-insulator transition in La_{2-x}Sr_xCuO₄ at the pair quantum resistance, *Nature* **472**, 458 (2011).
 - [10] K. Ueno, S. Nakamura, H. Shimotani, H. T. Yuan, N. Kimura, T. Nojima, H. Aoki, Y. Iwasa, and M. Kawasaki, Discovery of superconductivity in KTaO₃ by electrostatic carrier doping, *Nat. Nanotechnol.* **6**, 408 (2011).
 - [11] E. McCann, Asymmetry gap in the electronic band structure of bilayer graphene, *Phys. Rev. B* **74**, 161403(R) (2006).
 - [12] E. V. Castro, K. S. Novoselov, S. V. Morozov, N. M. R. Peres, J. M. B. Lopes dos Santos, J. Nilsson, F. Guinea, A. K. Geim, and A. H. Castro Neto, Biased Bilayer Graphene: Semiconductor with a Gap Tunable by the Electric Field Effect, *Phys. Rev. Lett.* **99**, 216802 (2007).
 - [13] K. I. Bolotin, K. J. Sikes, Z. Jiang, M. Klima, G. Fudenberg, J. Hone, P. Kim, and H. L. Stormer, Ultrahigh electron mobility in suspended graphene, *Solid State Commun.* **146**, 351 (2008).
 - [14] Y. Guo, W. Guo, and C. Chen, Tuning field-induced energy gap of bilayer graphene via interlayer spacing, *Appl. Phys. Lett.* **92**, 243101 (2008).

- [15] S. Konabe and S. Okada, Robustness and fragility of a linear dispersion band of bilayer graphene under an electric field, *J. Phys. Soc. Jpn.* **81**, 113702 (2012).
- [16] M. Otani and S. Okada, Field-induced free-electron carriers in graphite, *J. Phys. Soc. Jpn.* **79**, 073701 (2010).
- [17] M. Posternak, A. Baldereschi, A. J. Freeman, E. Wimmer, and M. Weinert, Prediction of Electronic Interlayer States in Graphite and Reinterpretation of Alkali Bands in Graphite Intercalation Compounds, *Phys. Rev. Lett.* **50**, 761 (1983).
- [18] M. Posternak, A. Baldereschi, A. J. Freeman, and E. Wimmer, Prediction of Electronic Surface States in Layered Materials: Graphite, *Phys. Rev. Lett.* **52**, 863 (1984).
- [19] A. K. Geim and I. V. Grigorieva, Van der Waals heterostructures, *Nature* **499**, 419 (2013).
- [20] M. Koshino and T. Ando, Orbital diamagnetism in multilayer graphenes: Systematic study with the effective mass approximation, *Phys. Rev. B* **76**, 085425 (2007).
- [21] M. Koshino and T. Ando, Magneto-optical properties of multilayer graphene, *Phys. Rev. B* **77**, 115313 (2008).
- [22] M. Otani, M. Koshino, Y. Takagi, and S. Okada, Intrinsic magnetic moment on (0001) surfaces of rhombohedral graphite, *Phys. Rev. B* **81**, 161403(R) (2010).
- [23] M. Otani, M. Koshino, Y. Takagi, and S. Okada, Phase control of magnetic state of graphite thin films by electric field, *Appl. Phys. Lett.* **96**, 242504 (2010).
- [24] Y. Gao, M. Maruyama, and S. Okada, Influence of interlayer stacking arrangements on carrier accumulation in bilayer graphene field effect transistors, *Appl. Phys. Express* **13**, 065006 (2020).
- [25] Y. Sakai, S. Saito, and M. L. Cohen, First-principles study on graphene/hexagonal boron nitride heterostructures, *J. Phys. Soc. Jpn.* **84**, 121002 (2015).
- [26] Y. Sakai, S. Saito, and M. L. Cohen, Electronic properties of B-C-N ternary kagome lattices, *Phys. Rev. B* **91**, 165434 (2015).
- [27] C.-H. Lee, G.-H. Lee, A. M. van der Zande, W. Chen, Y. Li, M. Han, X. Cui, G. Arefe, C. Nuckolls, T. F. Heinz, *et al.*, Atomically thin *p-n* junctions with van der Waals heterointerfaces, *Nat. Nanotechnol.* **9**, 676 (2014).
- [28] P. Rivera, J. R. Schaibley, A. M. Jones, J. S. Ross, S. Wu, G. Aivazian, P. Klement, K. Seyler, G. Clark, N. J. Ghimire, *et al.*, Observation of long-lived interlayer excitons in monolayer MoSe₂-WSe₂ heterostructures, *Nat. Commun.* **6**, 6242 (2015).
- [29] K. Zhang, T. Zhang, G. Cheng, T. Li, S. Wang, W. Wei, X. Zhou, W. Yu, Y. Sun, P. Wang, *et al.*, Interlayer transition and infrared photodetection in atomically thin type-II MoTe₂/MoS₂ van der Waals heterostructures, *ACS Nano* **10**, 3852 (2016).
- [30] K. Wang, B. Huang, M. Tian, F. Ceballos, M.-W. Lin, M. Mahjouri-Samani, A. Boulesbaa, A. A. Puzos, C. Rouleau, M. Yoon, *et al.*, Interlayer coupling in twisted WSe₂/WS₂ bilayer heterostructures revealed by optical spectroscopy, *ACS Nano* **10**, 6612 (2016).
- [31] D. Kozawa, A. Carvalho, I. Verzhbitskiy, F. Giustiniano, Y. Miyauchi, S. Mouri, A. H. Castro Neto, K. Matsuda, and G. Eda, Evidence for fast interlayer energy transfer in MoSe₂/WS₂ heterostructures, *Nano Lett.* **16**, 4087 (2016).
- [32] S. Mouri, W. Zhang, D. Kozawa, Y. Miyauchi, G. Eda, and K. Matsuda, Thermal dissociation of inter-layer excitons in MoS₂/MoSe₂ hetero-bilayers, *Nanoscale* **9**, 6674 (2017).
- [33] M. Z. Bellus, M. Li, S. D. Lane, F. Ceballos, Q. Cui, X. C. Zeng, and H. Zhao, Type-I van der Waals heterostructure formed by MoS₂ and ReS₂ monolayers, *Nanoscale Horiz.* **2**, 31 (2017).
- [34] T. Yamaoka, H. E. Lim, S. Koirala, K. Shinokita, M. Maruyama, S. Okada, Y. Miyauchi, and K. Matsuda, Efficient photocarrier transfer and effective photoluminescence enhancement in type I monolayer MoTe₂/WSe₂ heterostructure, *Adv. Funct. Mater.* **28**, 1801021 (2018).
- [35] E. Suárez Morell, J. D. Correa, P. Vargas, M. Pacheco, and Z. Barticevic, Flat bands in slightly twisted bilayer graphene: Tight-binding calculations, *Phys. Rev. B* **82**, 121407(R) (2010).
- [36] R. Bistritzer and A. H. MacDonald, Moiré bands in twisted double-layer graphene, *Proc. Natl. Acad. Sci. USA* **108**, 12233 (2011).
- [37] Y. Cao, V. Fatemi, S. Fang, K. Watanabe, T. Taniguchi, E. Kaxiras, and P. Jarillo-Herrero, Unconventional superconductivity in magic-angle graphene superlattices, *Nature* **556**, 43 (2018).
- [38] M. Maruyama, K. Nagashio, and S. Okada, Influence of interlayer stacking on gate-induced carrier accumulation in bilayer MoS₂, *ACS Appl. Electron. Mater.* **2**, 1352 (2020).
- [39] Y. Morikawa, K. Iwata, and K. Terakura, Theoretical study of hydrogenation process of formate on clean and Zn deposited Cu(111) surfaces, *Appl. Surf. Sci.* **169–170**, 11 (2001).
- [40] <https://state-doc.readthedocs.io/en/latest/index.html>.
- [41] P. Hohenberg and W. Kohn, Inhomogeneous electron gas, *Phys. Rev.* **136**, B864 (1964).
- [42] W. Kohn and L. J. Sham, Self-consistent equations including exchange and correlation effects, *Phys. Rev.* **140**, A1133 (1965).
- [43] J. P. Perdew, K. Burke, and M. Ernzerhof, Generalized Gradient Approximation Made Simple, *Phys. Rev. Lett.* **77**, 3865 (1996).
- [44] J. P. Perdew, K. Burke, and M. Ernzerhof, Generalized Gradient Approximation Made Simple [Phys. Rev. Lett. 77, 3865 (1996)], *Phys. Rev. Lett.* **78**, 1396 (1997).
- [45] D. S. Koda, F. Bechstedt, M. Marques, and L. K. Teles, Tuning electronic properties and band alignments of phosphorene combined with MoSe₂ and WSe₂, *J. Phys. Chem. C* **121**, 3862 (2017).
- [46] K. Lee, É. D. Murray, L. Kong, B. I. Lundqvist, and D. C. Langreth, Higher-accuracy van der Waals density functional, *Phys. Rev. B* **82**, 081101(R) (2010).
- [47] V. R. Cooper, Van der Waals density functional: An appropriate exchange functional, *Phys. Rev. B* **81**, 161104(R) (2010).
- [48] D. Vanderbilt, Soft self-consistent pseudopotentials in a generalized eigenvalue formalism, *Phys. Rev. B* **41**, 7892 (1990).
- [49] M. Otani and O. Sugino, First-principles calculations of charged surfaces and interfaces: A plane-wave nonrepeated slab approach, *Phys. Rev. B* **73**, 115407 (2006).
- [50] See the Supplemental Material at <http://link.aps.org/supplemental/10.1103/PhysRevApplied.14.044028> for the electronic structures of van der Waals heterostructures of MoS₂/WS₂ with a twisted arrangement.
- [51] M. Maruyama and S. Okada, Asymmetric carrier accumulation in van der Waals heterostructures of MoS₂/WS₂

- under an external electric field, *Appl. Phys. Express* **12**, 075008 (2019).
- [52] T. Chu, H. Ilatikhameneh, G. Klimeck, R. Rahman, and Z. Chen, Electrically tunable bandgaps in bilayer MoS₂, *Nano Lett.* **15**, 8000 (2015).
- [53] H. Yuan, H. Shimotani, J. Ye, S. Yoon, H. Allah, A. Tsukazaki, M. Kawasaki, and Y. Iwasa, Electrostatic and electrochemical nature of liquid-gated electric-double-layer transistors based on oxide semiconductors, *J. Am. Chem. Soc.* **132**, 18402 (2019).
- Correction:* The previously published Figure 3 was incorrect and has been replaced.